Inorganic Chemistry
Article

Inorg. Chem. **2010**, *49*, 5003–5008 **5003**
DOI: 10.1021/ic100108h

Investigation on the Protonation of a Trisubstituted $[Fe_2(CO)_3(PPh_3)(\kappa^2\text{-phen})(\mu\text{-pdt})]$ Complex: Rotated versus Unrotated Intermediate Pathways

Pierre-Yves Orain, Jean-François Capon, Frédéric Gloaguen, François Y. Pétillon, Philippe Schollhammer,* and Jean Talarmin

Université Européenne de Bretagne, France, and CNRS, UMR 6521 "Chimie, Electrochimie Moléculaires et Chimie Analytique", ISSTB, CS 29238 Brest-Cedex 3, France

Giuseppe Zampella and Luca De Gioia*

Department of Biotechnology and Bioscience, University of Milano−Bicocca, Piazza della Scienza 1, 20126 Milan, Italy

Thierry Roisnel

Centre de Diffractométrie X, UMR CNRS 6226, Université de Rennes 1, 35042 Rennes Cedex, France

Received January 18, 2010

The substitution of PPh_3 for a carbonyl group at the $\{Fe(CO)_3\}$ moiety in $[Fe_2(CO)_4(\kappa^2\text{-phen})(\mu\text{-pdt})]$ results in the formation of the trisubstituted complex $[Fe_2(CO)_3(PPh_3)(\kappa^2\text{-phen})(\mu\text{-pdt})]$ (**2**). Unlike its tetracarbonyl precursor, the protonation of **2** at low temperature does not afford any apparent transient terminal hydride species. Hydride formation for $[Fe_2(CO)_3(L)(\kappa^2\text{-phen})(\mu\text{-pdt})]$ (L = PPh_3, CO) species is also studied by density functional theory calculations, which show that activation barriers to give terminal and bridging hydrides can be remarkably close for this class of organometallic compounds.

Introduction

Mimics of the diiron subsite of [FeFe]-hydrogenases (Scheme 1) continue to be intensively developed because, until now, few efficient electrocatalysts have been obtained and the mechanism of the natural production/uptake of hydrogen remains unclear.[1]

It is obvious that a fine-tuning of the structural and electronic features of the coordination sphere of synthetic diiron molecules is required to improve their activity toward protons. Novel structural and chemical models are still necessary to gain a better understanding of the protonation mechanisms implied at the molecular level. Recently, the use of chelating ligands allowed better control of the steric and electronic properties of the artificial diiron framework. New models of the general formula $[Fe_2(CO)_4(\kappa^2\text{-}L_2)(\mu\text{-dithiolate})]$[2−7] and $[Fe_2(CO)_2(\kappa^2\text{-}L_2)_2(\mu\text{-dithiolate})]$[8] were synthesized in order to stabilize terminal hydride species that could act as possible key intermediates in the natural reversible hydrogen activation processes. Barton and Rauchfuss[8] demonstrated that two chelating diphosphines in diiron molecules $[Fe_2(CO)_2(\kappa^2\text{-}L_2)_2(\mu\text{-dithiolate})]$ (dithiolate = pdt, adt; L = dppv = *cis*-$Ph_2PCH{=}CHPPh_2$) inhibit the isomerization of terminal hydride into bridging hydride because of both the high basicity of the diiron center and the steric crowding of the diphosphine, while monochelated compounds $[Fe_2(CO)_4(\kappa^2\text{-}L_2)(\mu\text{-dithiolate})]$ underwent fast isomerization of terminal to bridging hydride even at temperature below −30 °C.[2,3,4a−c] Considering the few studies dedicated to

*To whom correspondence should be addressed. E-mail: schollha@univ-brest.fr (P.S.), luca.degioia@unimib.it (L.D.G.).

(1) (a) Capon, J.-F.; Gloaguen, F.; Pétillon, F. Y.; Schollhammer, P.; Talarmin, J. *Coord. Chem. Rev.* **2009**, *253*, 1476–1494. (b) Tard, C.; Pickett, C. J. *Chem. Rev.* **2009**, *109*, 2245–2274. (c) Gloaguen, F.; Rauchfuss, T. B. *Chem. Soc. Rev.* **2009**, *38*, 100–108. (d) Rakowski DuBois, M.; DuBois, D. L. *Chem. Soc. Rev.* **2009**, *38*, 62–72. (e) Felton, G. A. N.; Mebi, C. A.; Petro, B. J.; Vannucci, A. K.; Evans, D. H.; Glass, R. S.; Lichtenberger, D. L. *J. Organomet. Chem.* **2009**, *694*, 2681–2699. (f) Capon, J.-F.; Gloaguen, F.; Pétillon, F. Y.; Schollhammer, P.; Talarmin, J. *C.R. Chimie* **2008**, *11*, 842–851. (g) Capon, J.-F.; Gloaguen, F.; Pétillon, F. Y.; Schollhammer, P.; Talarmin, J. *Eur. J. Inorg. Chem.* **2008**, 4671–4681.

(2) Orain, P.-Y.; Capon, J.-F.; Kervarec, N.; Gloaguen, F.; Pétillon, F.; Pichon, R.; Schollhammer, P.; Talarmin, J. *Dalton Trans.* **2007**, 3754–3756.

(3) Morvan, D.; Capon, J.-F.; Gloaguen, F.; Le Goff, A.; Marchivie, M.; Michaud, F.; Schollhammer, P.; Talarmin, J.; Yaouanc, J.-J. *Organometallics* **2007**, *26*, 2042–2052.

Published on Web 05/05/2010

Scheme 1

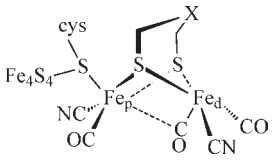

trisubstituted molecules of the general formula $[Fe_2(CO)_3L_3(\mu\text{-dithiolate})]$[5,9,10] that can be proposed as models mimicking the dithiolate diiron tricarbonyl center of the natural diiron $[2Fe]_H$ subsite, we decided to investigate the protonation of $[Fe_2(CO)_3L'(\kappa^2\text{-}L_2)(\mu\text{-dithiolate})]$ in order to verify that the combination of a chelated ligand at one iron site with a phosphine group located at the other metallic site could provide sufficient basicity at the $\{Fe(CO)_2L\}$ moiety for stabilizing a terminal hydride compound. Recently, Hogarth and Richards reported the synthesis and protonation of the triphosphine complex $[Fe_2(CO)_3\{\mu,\kappa^2\text{-}(Ph_2PCH_2CH_2)_2PPh\}(\mu\text{-pdt})]$ at room temperature, giving a bridging hydride compound.[9] More recently, NMR and theoretical studies of the protonation process of complexes $[Fe_2(CO)_{4-x}L_x(\kappa^2\text{-dppv})(\mu\text{-pdt})]$ ($x = 0, 1$; L = PMe_3) were reported by De Gioia and Rauchfuss.[10] Their studies suggest a general pathway for the protonation process of the diiron bridging dithiolate molecules, implying a transient terminal hydride intermediate. This prompts us to complete our ongoing works concerning the chemical effect of the replacement of a carbonyl by a phosphine at the $\{Fe(CO)_3\}$ moiety on the protonation process in dissymmetrically substituted monochelated compounds. To support this experimental work, we present also a theoretical study of the protonation of $[Fe_2(CO)_{4-x}L_x(\kappa^2\text{-phen})(\mu\text{-pdt})]$ complexes ($x = 0, 1$; L = PPh_3 or PMe_3), in which the electron-donating phenanthroline ligand prevents the formation of basal−apical isomers, which limits the analysis to a dibasal form.[2]

Scheme 2

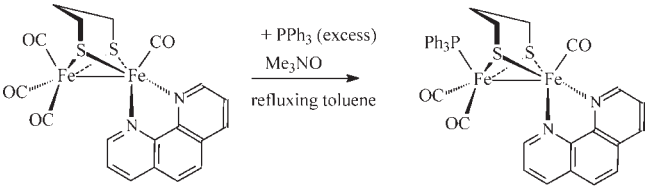

1 **2**

Results and Discussion

Synthesis, Characterization, and Protonation Study of $[Fe_2(CO)_3(PPh_3)(\kappa^2\text{-phen})(\mu\text{-pdt})]$ (2). The treatment of $[Fe_2(CO)_4(\kappa^2\text{-phen})(\mu\text{-pdt})]$ (**1**) with an excess of PPh_3 in refluxing toluene in the presence of $Me_3NO\cdot 2H_2O$ afforded the expected PPh_3-substituted complex **2** in low yields after chromatography (Scheme 2). The $^{31}P\{^1H\}$ NMR spectrum in CD_2Cl_2 displays a singlet at 59.3 ppm, and the ^1H NMR data (see the Experimental Section) are in accordance with the replacement of one PPh_3 for CO. The IR spectrum, recorded in toluene, exhibits three bands in the ν_{CO} region at 1950, 1897, and 1880 cm^{-1}, which are shifted to lower energies by ca. 39 cm^{-1} relative to those of **1**, which is consistent with the electron-donating effect of the phosphine ligand. Several attempts to perform X-ray analysis on different samples of crystals of **2** cannot be considered satisfactory (see Figure 1 in the Supporting Information). The most that can be said is that the X-ray results are consistent with the chemical and spectroscopic evidence, which indicates the formation of **2** with a dibasal binding mode of the phenanthroline group and an apical position of the PPh_3 ligand, as has been shown for complexes $[Fe_2(\mu\text{-pdt})(dppv)(PMe_3)(CO)_3]$ and $(Et_4N)[Fe_2(\mu\text{-pdt})(dppv)(CN)(CO)_3]$.[5]

The treatment of **2** with an excess of $HBF_4\cdot OEt_2$ (5 equiv) at 183 K led to the straightforward formation of a bridging hydride species $[Fe_2(CO)_3(PPh_3)(\kappa^2\text{-phen})(\mu\text{-pdt})(\mu\text{-H})]^+$ (**3**; Scheme 3). No intermediate with a terminal hydride was detected in this reaction.

The ^1H NMR spectrum of **3** in CD_2Cl_2 at 183 K exhibits two doublets at −7.69 and −9.37 ppm with typical coupling constants[11] J_{PH} of 25.6 and 13.0 Hz, respectively (Figure 2 in the Supporting Information). These signals can be confidently assigned to basal ($\mathbf{3_{ba}}$) and apical ($\mathbf{3_{ap}}$) isomers, respectively.[10b] The warming of the solution at room temperature revealed a typical apical−basal isomerization of $\mathbf{3_{ap}}$ into $\mathbf{3_{ba}}$ (Scheme 3).[4]

The IR spectrum of a CH_2Cl_2 solution of **3**, obtained at room temperature by the addition of 5 equiv of $HBF_4\cdot OEt_2$ to **2**, exhibits three strong bands in the ν_{CO} region at 2036, 1984, and 1967 cm^{-1}, which are similar to those observed for the related bridging hydride compound $[Fe_2(CO)_3\{\mu,\kappa^2\text{-}(Ph_2PCH_2CH_2)_2PPh\}(\mu\text{-pdt})\ (\mu\text{-H})]^+$[9] (Figure 3 in the Supporting Information). Unfortunately, like its carbonyl analogue $[Fe_2(CO)_4(\kappa^2\text{-phen})(\mu\text{-pdt})(\mu\text{-H})]^+$ (**4**),[2] **3** was unstable at room temperature and no reliable elemental analysis and single crystal could be obtained. This led us to try to crystallize compound **4** at low temperature. As a matter of fact, single crystals of **4** were successfully grown by the slow diffusion of pentane

(4) (a) Ezzaher, S.; Capon, J.-F.; Gloaguen, F.; Pétillon, F. Y.; Schollhammer, P.; Talarmin, J.; Pichon, R.; Kervarec, N. *Inorg. Chem.* **2007**, *46*, 3426–3428. (b) Adam, F. I.; Hogarth, G.; Kabir, S. E.; Richards, I. *C.R. Chimie* **2008**, *11*, 890–905. (c) Ezzaher, S.; Capon, J.-F.; Gloaguen, F.; Pétillon, F. Y.; Schollhammer, P.; Talarmin, J.; Pichon, R.; Kervarec, N. *C.R. Chimie* **2008**, *11*, 906–914. (d) Ezzaher, S.; Capon, J.-F.; Gloaguen, F.; Pétillon, F. Y.; Schollhammer, P.; Talarmin, J. *Inorg. Chem.* **2007**, *46*, 9863–9872. (e) Wang, N.; Wang, M.; Liu, T.; Zhang, T.; Darensbourg, M. Y.; Sun, L. *Inorg. Chem.* **2008**, *47*, 6948–6955. (f) Adam, F. I.; Hogarth, G.; Richards, I.; Sanchez, B. E. *Dalton Trans.* **2007**, 2495–2498. (g) Duan, L.; Wang, M.; Li, P.; Na, Y.; Wang, N.; Sun, L. *Dalton Trans.* **2007**, 1277–1283. (h) Morvan, D.; Capon, J.-F.; Gloaguen, F.; Pétillon, F. Y.; Schollhammer, P.; Talarmin, J.; Yaouanc, J.-J; Michaud, F.; Kervarec, N. *J. Organomet. Chem.* **2009**, *694*, 2801–2807. (i) Ezzaher, S.; Capon, J.-F.; Dumontet, N.; Gloaguen, F.; Pétillon, F. Y.; Schollhammer, P.; Talarmin, J. *J. Electroanal. Chem.* **2009**, *626*, 161–170. (j) Song, L.-C.; Wang, T.-H.; Ge, J.-H.; Mei, S.-Z.; Gao, J.; Wang, L.-X.; Gai, B.; Zhao, L.-Q.; Yan, J.; Wang, Y.-Z. *Organometallics* **2008**, *27*, 1409–1416. (k) Harb, M. K.; Windhager, J.; Daraosheh, A.; Görls, H.; Lockett, L. T.; Okumura, N.; Evans, D. H.; Glass, R. S.; Lichtenberger, D. L.; El-Khateeb, M.; Weigand, W. *Eur. J. Inorg. Chem.* **2009**, 3414–3420.

(5) Justice, A. K.; Zampella, G.; De Gioia, L.; Rauchfuss, T. B.; van der Vlugt, J. I.; Wilson, S. R. *Inorg. Chem.* **2007**, *46*, 1655–1664.

(6) Ezzaher, S.; Orain, P.-Y.; Capon, J.-F.; Gloaguen, F.; Pétillon, F. Y.; Roisnel, T.; Schollhammer, P.; Talarmin, J. *Chem. Commun.* **2008**, 2547–2549.

(7) (a) Ezzaher, S.; Capon, J.-F.; Gloaguen, F.; Pétillon, F. Y.; Schollhammer, P.; Talarmin, J.; Kervarec, N. *Inorg. Chem.* **2009**, *48*, 2–4. (b) Wang, N.; Wang, M.; Zhang, T.; Li, P.; Liu, J.; Sun, L. *Chem. Commun.* **2008**, 5800–5802.

(8) Barton, B. E.; Rauchfuss, T. B. *Inorg. Chem.* **2008**, *47*, 2261–2263.

(9) Hogarth, G.; Richards, I. *Inorg. Chem. Commun.* **2007**, *10*, 66–70.

(10) (a) Zampella, G.; Fantucci, P.; De Gioia, L. *J. Am. Chem. Soc.* **2009**, *131*, 10909–10917. (b) Barton, B. E.; Zampella, G.; Justice, A. K.; De Gioia, L.; Rauchfuss, T. B.; Wilson, S. R. *Dalton Trans.* **2010**, 3011–3019.

(11) van der Vlugt, J. I.; Rauchfuss, T. B.; Whaley, C. M.; Wilson, S. R. *J. Am. Chem. Soc.* **2005**, *127*, 16002–16013.

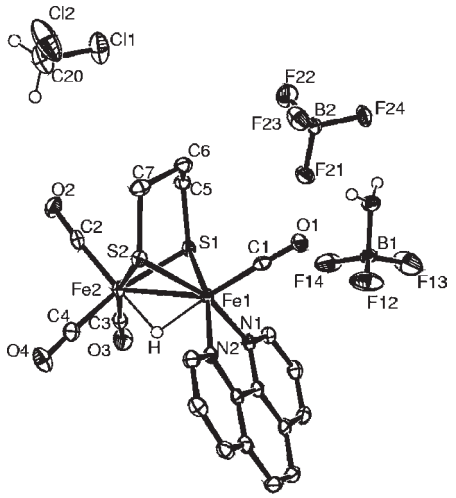

Figure 1. Molecular structure of compound $[Fe_2(CO)_4(\kappa^2\text{-phen})(\mu\text{-pdt})(\mu\text{-H})](BF_4)$, CH_2Cl_2, and $H_2O\cdot BH_3$ (**4**) with thermal ellipsoids at 30% probability.

Scheme 3

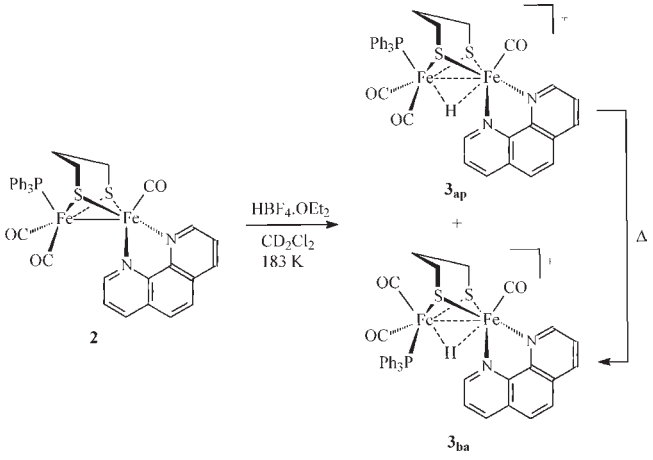

Table 1. Selected Bond Lengths (Å) and Angles (deg) for **4**

Fe1−Fe2	2.5990(5)	Fe2−S2	2.2867(7)
Fe1−N1	1.998(2)	Fe2−H	1.59(3)
Fe1−N2	1.997(2)	C1−O1	1.144(3)
Fe1−S1	2.2252(7)	C2−O2	1.135(3)
Fe1−S2	2.2422(7)	C3−O3	1.134(3)
Fe1−H	1.77(3)	C4−O4	1.134(3)
Fe1−C1	1.780(3)		
Fe2−C2	1.815(3)	Fe1−S1−Fe2	70.37(2)
Fe2−C3	1.817(3)	Fe1−S2−Fe2	70.03(2)
Fe2−C4	1.825(3)		
Fe2−S1	2.2842(7)		

into dichloromethane at 213 K, which allowed us to describe the structure of one member of the series of complexes $[Fe_2(CO)_3L(\kappa^2\text{-phen})(\mu\text{-pdt})(\mu\text{-H})]^+$ (Figure 1 and Table 1). The main feature of this structure is the unsymmetrical binding mode of the hydride [Fe1−H, 1.77(3) Å; Fe2−H, 1.59(3) Å], which is similar to that observed in the bis-N-heterocyclic carbene analogue $[Fe_2(CO)_4(\eta^2\text{-}I_{Me}CH_2I_{Me})(\mu\text{-pdt})(\mu\text{-H})]^+$ (where $I_{Me}CH_2I_{Me}$ = 1,3-dimethylimidazol-2-ylidene; Fe−H, 1.710 and 1.562 Å).[3]

The substitution of PPh_3 for a carbonyl ligand at the $\{Fe(CO)_3\}$ moiety in the trisubstituted complex **2** does not stabilize, even at low temperature, any transient terminal hydride species. This led us to wonder if the process affording the bridging hydride diiron derivative operates systematically through an initial formation of a transient terminal hydride species. Moreover, no terminal hydride species was detected at 188 K in the ^1H NMR spectrum of the tetracarbonyl edt analogue of **1**, $[Fe_2(CO)_4(\kappa^2\text{-phen})(\mu\text{-edt})]$, in the presence of a weaker acid than HBF_4,[2,4a] such as CF_3CO_2H, but the straightforward formation of a bridging hydride derivative was observed. The protonation of **1** with HBF_4 in the same reaction conditions affords a terminal hydride species that isomerizes at higher temperature. Similar results have been obtained in the reaction of the related diphosphine compound $[Fe_2(CO)_4(\kappa^2\text{-dppe})(\mu\text{-pdt})]$ with CF_3CO_2H. This might suggest that the protonation at the inverted iron center in the rotated transition state requires the use of a sufficiently strong acid; otherwise, it is the unrotated form that is protonated at the bridging site.

Scheme 4. Computed Energy Profile for the Formation of Terminal Hydride and μ-Hydride Derivatives for Complex **2**[a]

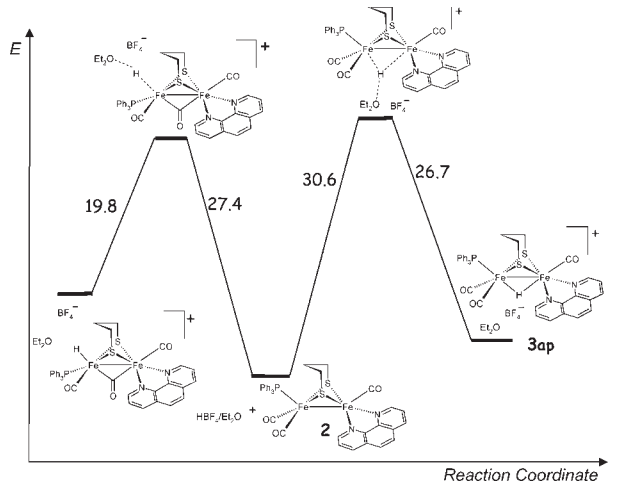

[a] Energies are in kcal/mol. All structures can be drawn showing the central carbon atom of the dithiolate ligand directed either at the open coordination site or away from that site. Because the two forms were computed to be very close in energy, we arbitrarily decided to draw the structures in the first fashion.

Scheme 5. Computed Energy Profile for the Formation of Terminal Hydride and μ-Hydride Derivatives for Complex **2**, When F_3CSO_3H (Triflic Acid) Is Employed as a Proton-Releasing System[a]

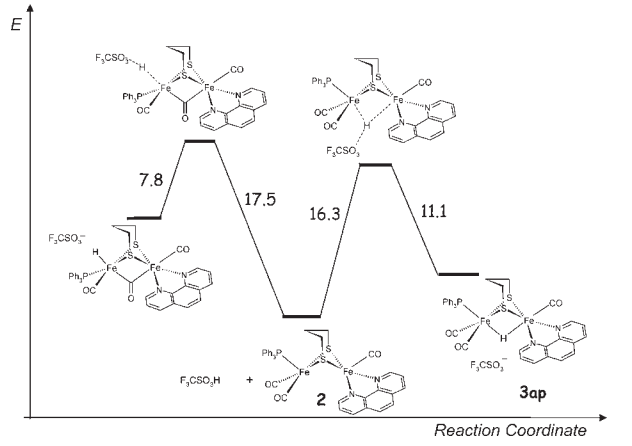

[a] Energies in kcal/mol.

Scheme 6. Rearrangement of the $(CO)_2L$ Ligands Leading to $[Fe_2(CO)_3(L)(\kappa^2\text{-phen})(\mu\text{-pdt})]$ (L = PPh_3, CO) Forms Featuring a Terminal Vacant Coordination Position

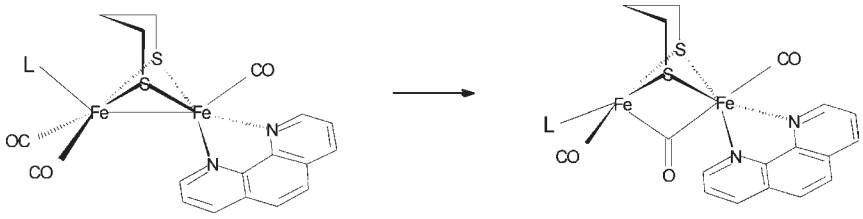

Scheme 7. Computed Energy Profile for the Formation of Terminal Hydride and μ-Hydride Derivatives for the $[Fe_2(CO)_3(PMe_3)(\kappa^2\text{-phen})(\mu\text{-pdt})]$ Complex[a]

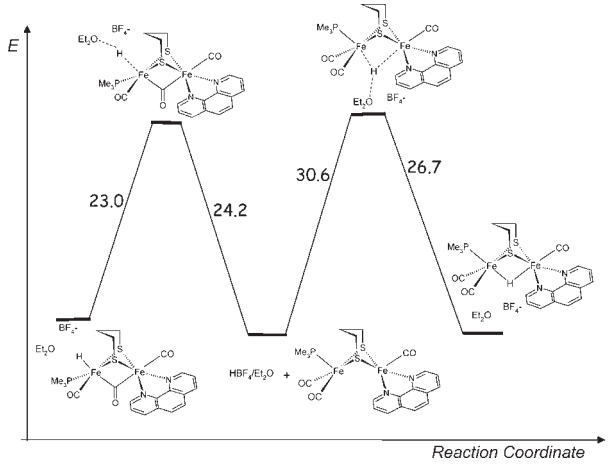

[a] Energies are in kcal/mol.

Scheme 8. Computed Energy Profile for the Formation of Terminal Hydride and μ-Hydride Derivatives for Complex **2**, When F_3CSO_3H Is Employed as the Proton-Releasing System[a]

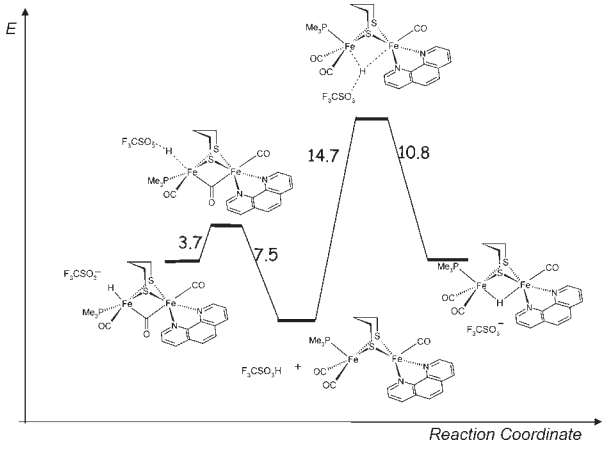

[a] Energies are in kcal/mol.

To strengthen the understanding of the protonation processes discussed above, we used density functional theory (DFT) calculations to dissect the reaction between $[Fe_2(CO)_3(L)(\kappa^2\text{-phen})(\mu\text{-pdt})]$ (L = PPh_3, PMe_3, CO) and typical acids such as $HBF_4\cdot OEt_2$ or CF_3SO_3H. According to the DFT results, the μ-hydride species **3** is lower in energy than the corresponding terminal hydride isomer (Scheme 4). In addition, the basal form $\mathbf{3_{ba}}$ is computed to be thermodynamically more stable than the corresponding apical $\mathbf{3_{ap}}$ isomer (not shown), in agreement with experimental observations. The reaction energy barriers that were calculated for the protonation of **2** by $HBF_4\cdot OEt_2$ are quite large (27.4 and 30.6 kcal/mol; Scheme 4), and they differ only by 3.2 kcal/mol. In particular, DFT calculations would suggest that the terminal protonation of **2** is kinetically slightly preferred to μ protonation, in contradiction with experimental evidence. However, it must be noted that the difference between the reaction energy barriers is close to the expected error of the method for such kinds of calculations and, most importantly, the description within the DFT representation of the acid moiety $HBF_4\cdot OEt_2$ might be nonoptimal. In fact, it is known that the proper description of the chemical nature of the $HBF_4\cdot OEt_2$ species in solution can be difficult.[12]

To try to overcome modeling limitations, we have also computed the reaction energy profile for the protonation of **2** using CF_3SO_3H as the acid moiety (Scheme 5). Remarkably, when CF_3SO_3H is the acid, it turns out that μ protonation is the most kinetically favored pathway, even though the reaction energy barriers for terminal protonation and μ-protonation are still very similar (16.3 and 17.5 kcal/mol for μ-protonation and terminal protonation, respectively). In this context, it must be noted that previous DFT investigations of terminal protonation versus μ-protonation in diiron complexes containing phosphine ligands[10a] showed that terminal protonation is generally clearly favored relative to μ protonation. This latter observation prompted us to further investigate the protonation mechanism of **2**, with the aim of better highlighting the electronic and steric factors responsible of its peculiar behavior. First we have taken into account the possibility that terminal hydride formation takes place on going through a stepwise mechanism, which implies an initial rotation of the $Fe(CO)_2(PPh_3)$ moiety, leading to a species featuring a vacant coordination site suited to react with the acid and form the terminal hydride (Scheme 6). Indeed, it turned out that the rotated species **2** does not correspond to a stable species but to a transition state, excluding the possibility of a stepwise protonation mechanism. Nevertheless, it is worth noting that the computed energy barrier for the rotation of $Fe(CO)_2(PPh_3)$ in **2** is very low (4.6 kcal/mol) and similar to the corresponding value computed for the rotation of the $Fe(CO)_3$ moiety in **1**, clearly showing how the stereoelectronic properties of the PPh_3 group do not hinder the rotation process. This result suggests that the kinetically hindered event during the terminal protonation of **2** is not the rearrangement of the ligands coordinated to the iron atom but the proton

(12) Greenwood, N. N.; Earnshaw, A. *Chemistry of Elements*; 2nd ed.; Butterworth Heinemann (Elsevier Science): Linacre House, Jordan Hill, Oxford, 1997; p 199.

Scheme 9. Computed Energy Profile for the Formation of Terminal and μ-Hydride Derivatives for Complex **1**[a]

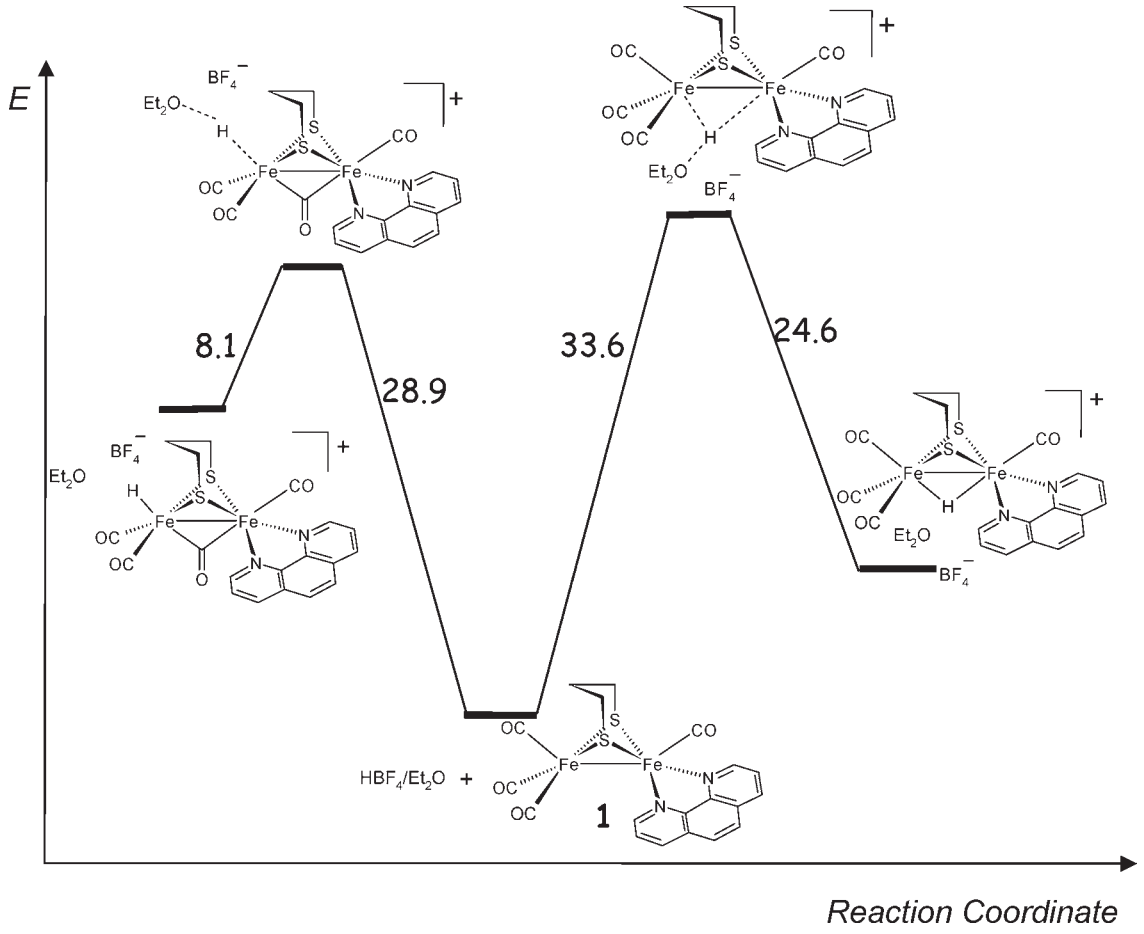

[a] Energies are in kcal/mol.

transfer from the acid to the diiron complex. Therefore, to further shed light on the factors affecting the terminal protonation in **2**, we have used again DFT methods to study the protonation of the $[Fe_2(CO)_3(PMe_3)(\kappa^2\text{-phen})(\mu\text{-pdt})]$ complex, which differs from **2** by the replacement of the PPh_3 ligand by the sterically less bulky PMe_3 group. We used both $HBF_4 \cdot OEt_2$ and CF_3SO_3H as proton sources (Schemes 7 and 8). Considering the reaction with $HBF_4 \cdot OEt_2$, it turns out that the energy barriers calculated for μ-protonation in $[Fe_2(CO)_3(PMe_3)(\kappa^2\text{-phen})(\mu\text{-pdt})]$ and **2** are very similar (29.0 and 30.6 kcal/mol, respectively), while that calculated for the terminal protonation in $[Fe_2(CO)_3(PMe_3)(\kappa^2\text{-phen})(\mu\text{-pdt})]$ is somewhat lower (24.2 kcal/mol) than that in **2** (27.4 kcal/mol). The kinetic preference for terminal protonation versus μ-protonation is even more evident when CF_3SO_3H is the acid. Indeed, in this case, the energy barriers for μ protonation of $[Fe_2(CO)_3(PMe_3)(\kappa^2\text{-phen})(\mu\text{-pdt})]$ and **2** are still similar (14.7 and 17.5 kcal/mol, respectively), whereas the corresponding energy barriers for terminal protonation differ by 10 kcal/mol (7.5 and 17.5 kcal/mol). The larger energy difference between the reaction energy barriers leading to terminal hydride and μ-hydride computed for $[Fe_2(CO)_3(PMe_3)(\kappa^2\text{-phen})(\mu\text{-pdt})]$, relative to that computed for **2**, can be rationalized by considering that steric accessibility to the Fe−Fe bond is essentially identical in the two diiron complexes, whereas that to the terminal coordination site is more hindered in **2** by the bulky PPh_3 ligand. The latter observations emphasize the critical role of the metal accessibility to implement the kinetics of the protonation in diiron complexes featuring phosphine and phenanthroline ligands. They also fit well with recently reported results that highlighted the crucial role of pendant acid/basic groups (such as an amine) within the diiron complex scaffold to increase the rate of protonation of bioinspired diiron complexes.[13]

The pathways for the formation of the μ-hydride and terminal hydride species in the reaction between **1** and $HBF_4 \cdot OEt_2$ have also been explored by DFT calculations (Scheme 9). The computed energy profile shows that in this case the route leading to the terminal hydride species is clearly kinetically favored because the corresponding activation energy is 4.7 kcal/mol lower than that calculated for the formation of the bridging hydride isomer. The fact that the reaction energy barriers computed for **1** are larger than those for **2** (28.9 and 33.6 kcal/mol versus 27.4 and 30.6 kcal/mol) can be explained by the replacement of CO with a PPh_3 group, which increases the basicity of the complex. Such an effect is even more evident when considering the relative thermodynamic stability of the hydride species. In fact, the terminal

(13) (a) Barton, B. E.; Olsen, M. T.; Rauchfuss, T. B. *J. Am. Chem. Soc.* **2008**, *130*, 16834–16835. (b) Wang, N.; Wang, M.; Liu, J.; Chen, L.; Sun, L. *Inorg. Chem.* **2009**, *48*, 11551–11558.

hydride [$HFe_2(CO)_4(\kappa^2$-phen)(μ-pdt)] is significantly higher in energy than the corresponding bridging hydride isomer (Scheme 9).

Conclusion

The replacement of a carbonyl by a phosphine at the {$Fe(CO)_3$} moiety in dissymmetrically substituted monochelated diiron compounds does not allow characterization of any terminal hydride species upon reaction with $HBF_4 \cdot OEt_2$, and only the corresponding bridging hydride isomer is observed. DFT calculations on the hydride formation for species **1** indicate that terminal hydride is the initial product, in agreement with the experimental observations, whereas for **2**, activation barriers for the formation of terminal and bridging hydrides are remarkably close and therefore the possibility of the direct formation of a bridging hydride cannot be excluded.

Experimental Section

Methods and Materials. All of the experiments were carried out under an inert atmosphere, using Schlenk techniques. [$Fe_2(CO)_4(\kappa^2$-phen)(μ-pdt)] (**1**) was prepared according to the reported procedure.[2] The NMR spectra (^{1}H and ^{31}P) were recorded at room temperature in a CD_2Cl_2 solution with a Bruker AMX 400, DRX 500, or AC300 spectrometer and were referenced to $SiMe_4$ (^{1}H NMR) and H_3PO_4 (^{31}P NMR). The IR spectra were recorded on a Nicolet Nexus Fourier transform spectrometer. Chemical analyses were made by the Service de Microanalyses ICSN, Gif sur Yvette, France.

Crystal data (Table 2) for **4** were collected at $T = 100$ K on a Bruker-AXS APEXII diffractometer, equipped with a jet cooler device and graphite-monochromated Mo Kα radiation (λ = 0.710 73 Å). The structure was solved by direct methods using the *SIR97* program[14a] and refined by least-squares methods based on F^2 with *SHELXL*.[14b]

Synthesis and Spectroscopic Data of [$Fe_2(CO)_3(PPh_3)(\kappa^2$-phen)($\mu$-pdt)] (2). A total of 1.040 g (2.0 mmol) of **1**, 1.604 g (6.1 mmol) of PPh_3, and 0.227 g (2.0 mmol) of $Me_3NO \cdot 2H_2O$ were stirred in refluxing toluene overnight. After filtration, the solvent was removed in vacuo. The product was purified by column chromatography on silica gel with CH_2Cl_2/hexane (60:40) as the eluent and washed with pentane. Yield: 0.175 g, 11.5%. IR (toluene, cm^{-1}): ν_{CO} 1950(s), 1897(s), 1880(s). ^{1}H NMR (CD_2Cl_2, 25 °C): δ 9.04 (dd, 2H, J_{HH} = 0.9 Hz, J_{HH} = 5.4 Hz, phen), 8.15 (d, 2H, J_{HH} = 0.9 Hz, J_{HH} = 7.9 Hz, phen), 7.86 (s, 2H, phen), 7.51 (dd, 2H, J_{HH} = 5.5 Hz, J_{HH} = 7.9 Hz, phen), 7.60 (m, 6H, PPh_3), 7.32 (m, 9H, PPh_3), 1.60 (m, 3H, pdt), 1.44 (m, 2H, pdt), 0.55 (m, 1H, pdt). ^{31}P{^{1}H} (CD_2Cl_2, 25 °C): δ 59.3. Anal. Calcd for $C_{36}H_{29}Fe_2N_2O_3PS_2,CH_2Cl_2$: C, 53.58; H, 3.77; N, 3.78. Found: C, 53.31; H, 3.77; N, 3.23.

DFT Calculations. DFT calculations have been carried out with the *TURBOMOLE 5.7* suite.[15] Geometry optimizations and transition-state searches have been carried out using the pure functional B-P86,[16] in conjunction with a valence triple-ζ basis set with polarization on all atoms, a level of theory that has been shown to be suited to reliably investigate [FeFe]-hydrogenase models.[17]

Stationary points of the energy hypersurface have been located by means of energy gradient techniques, and a full vibrational analysis has been carried out to further characterize each stationary point. Optimization of the transition state structures has been carried out according to a procedure based on a pseudo-Newton−Raphson method. Initially, geometry optimization of a guessed transition state structure is carried out, constraining the distance corresponding to the reaction coordinate. Vibrational analysis at the B-P86/TZVP level of the constrained minimum-energy structures is then carried out, and if one negative eigenmode corresponding to the reaction coordinate is found, the curvature determined at such a point is used as the starting point in the transition state search. The location of the transition state structure is carried out using an eigenvector-following search: the eigenvectors in the Hessian are sorted in ascending order, with the first one being that associated with the negative eigenvalue. After the first step, however, the search is performed by choosing the critical eigenvector with a maximum overlap criterion, which is based on the dot product with the eigenvector followed in the previous step.

The energies reported in the present contribution are pure electronic energies (E). In fact, the computation of classical corrections by means of evaluating the rotovibrational partition function, in order to have an estimate of the Gibbs free energy, did not afford, in the present case, significant variations to the reported energy profiles. Furthermore, COSMO corrections have also been tested by including the ϵ value corresponding to the experimentally adopted solvent (dichloromethane, ϵ = 9.1 at standard conditions of T and P). Because no appreciable changes to the whole energy profiles were observed, only in vacuo values are reported. In light of the available experimental data and considering the chemical nature of the ligands, only low-spin species have been investigated.

Table 2. Crystallographic Data for Complex **4**

empirical formula	$C_{20}H_{19}B_2Cl_2F_7Fe_2N_2O_5S_2$
fw	768.71
temperature (K)	100(2)
cryst syst	triclinic
space group	$P\bar{1}$
a (Å)	11.3463(7)
b (Å)	11.4918(7)
c (Å)	12.4419(8)
α (deg)	88.214(3)
β (deg)	64.190(3)
γ (deg)	81.344(3)
V (Å^3)	1442.75(16)
Z	2
ρ_{calcd} (Mg/mm^3)	1.770
μ (mm^{-1})	1.416
cryst size (mm)	0.54 × 0.34 × 0.27
range of θ (deg)	3.53−27.46
reflns measd	24 721
R_{int}	0.0427
unique data/param	6559/389
R1 [$I > 2\sigma(I)$]	0.0355
R1 (all data)	0.0534
wR2 (all data)	0.0876
GOF on F^2	1.030
$\Delta\rho_{max}$, $\Delta\rho_{min}$ (e/Å^3)	0.854, −0.931

Acknowledgment. The authors thank CNRS, ANR "CatH_2", UBO, and University of Milano−Bicocca for financial support. P.-Y.O. thanks ADEME for funding.

Supporting Information Available: Crystallographic data for **2** and **4**, NMR figures, tables giving *xyz* coordinates of optimized models, and a CIF file for compound **4**. This material is available free of charge via the Internet at http://pubs.acs.org.

(14) (a) *SIR97*: Altomare, A.; Burla, M. C.; Camalli, M.; Cascarano, G.; Giacovazzo, C.; Guagliardi, A.; Moliterni, A. G. G.; Polidori, G.; Spagna, R. *J. Appl. Crystallogr.* **1999**, *32*, 115–119. (b) Sheldrick, G. M. *Acta Crystallogr., Sect. A* **2008**, *64*, 112–122.

(15) (a) Ahlrichs, R.; Bar, M.; Haser, M.; Horn, H.; Kolmel, C. *Chem. Phys. Lett.* **1989**, *162*, 165–169. (b) Eichkornn, K.; Weigend, F.; Treutler, O.; Ahlrichs, R. *Theor. Chem. Acc.* **1997**, *97*, 119–124.

(16) (a) Becke, A. D. *Phys. Rev. A* **1988**, *38*, 3098–3100. (b) Perdew, J. P. *Phys. Rev. B* **1986**, *33*, 8822–8824.

(17) (a) Bertini, L.; Bruschi, M.; De Gioia, L.; Fantucci, P.; Greco, C.; Zampella, G. *At. Approaches Mod. Biol.: Quantum Chem. Mol. Simul.* **2007**, *268*, 1–46. (b) Bruschi, M.; Zampella, G.; Fantucci, P.; De Gioia, L. *Coord. Chem. Rev.* **2005**, *249*, 1620–1640. (c) Bruschi, M.; Greco, C.; Zampella, G.; Ryde, U.; Pickett, C. J.; De Gioia, L. *C.R. Chimie* **2008**, *11*, 834–841.